Petroleum Science 19 (2022) 731–742

Contents lists available at ScienceDirect

Petroleum Science

journal homepage: www.keaipublishing.com/en/journals/petroleum-science

Original Paper

Effect of structural parameters on the setting performance of plug slips during hydraulic fracturing

Chao Zheng [a, b, *], Zeng-Kai Liu [b], Xin-Lei Wu [b], Aibaibu Abulimiti [b], Jie Qin [b], Xue-Fei Zheng [b], Yong-Hong Liu [b]

[a] Department of Chemical and Process Engineering, University of Surrey, Guildford, GU2 7XH, United Kingdom
[b] College of Mechanical and Electronic Engineering, China University of Petroleum, Qingdao, 266580, China

ARTICLE INFO

Article history:
Received 24 August 2020
Accepted 6 January 2021
Available online 15 September 2021

Edited by Xiu-Qiu Peng

Keywords:
Hydraulic fracturing
Plug slips
Setting performance
Fracture failure

ABSTRACT

Slip is one of the most critical components for the frac plug, which would lodge into the casing and lock the frac plug in place during the setting and anchoring process. However, fracture failure of slip significantly affects the hydraulic fracturing effects and has attracted tremendous attention. In this paper, a three-dimensional contact model is applied to explore the setting process of slip. The effects of key structural parameters such as apex angle, inclination angle, and wedge angle on the contact characteristics of slip are systematically investigated. Numerical results indicate that the maximum contact stress appears at the contact area between slip tooth and the casing's inner wall. Besides, the maximum contact stress generally increases with the increase of apex angle and inclination angle, while decrease linearly with the rise in the wedge angle. Experimental results show that the slip teeth get blunt and appear severe plastic deformation, which arises from stress concentration. Comparison of biting area indicates that the experimental results are about 21.3% larger, which still have a reasonable agreement with the numerical results. These obtained results can guide the parametric selection of plug slip and other similar components.

1. Introduction

For the past decades, oil and gas resources have been treated as the most crucial energy source. With the fast consumption of oil and gas, unconventional reservoirs have been more and more popular for an alternative option (Ge et al., 2015; Wang et al., 2015; Mahmoodi et al., 2019). Generally, tight sands, coal beds, and shale formations are the most common unconventional oil and gas reservoirs (Rosine et al., 2008; Zheng et al., 2015; Tan et al., 2019; Vishkai and Gates, 2019). One distinct advantage of the unconventional oil and gas reservoir is the vast storage. However, the extra-low permeability feature has increased the difficulty of extracting the unconventional source. The development of drilling technology, well stimulation technology, and advanced downhole tools make the extraction of so-called unconventional oil and gas reservoirs technically and economically feasible (Rutqvist et al., 2013; Tong et al., 2019). Hydraulic fracturing technology, which was firstly introduced in 1947, has been widely applied to improve the permeability of oil and gas reservoirs.

The working principle for hydraulic fracturing is that using high-pressure fluid to create fractures in the formation (Zheng et al., 2016; Ai et al., 2018; Haddad and Kamy, 2019, Dong et al., 2020). Then, proppants are used to avoid the closure of fractures (Tsai et al., 2012; Suri et al., 2019). The fractures distributed in the formation help to improve the permeability dramatically. To improve extraction efficiency, horizontal well fracturing technology was proposed to extract low permeability reservoirs (Castro et al., 2013; Demarchos et al., 2005). Compared with conventional vertical well fracturing, horizontal wells offer a larger contact area with the oil and gas area (Cai et al., 2009). Besides, horizontal well fracturing contributes to more fractures along the horizontal section.

For horizontal well fracturing technology, the whole well is usually isolated for multiple stages with isolation tools. Frac plugs is a typical downhole isolation tool for horizontal multistage completions (Deshpande et al., 2012; Shaw, 2011; Hejl et al., 2007). During a plug operation, the frac plug assembly are pumped to the target position. Then, the frac plug is set with specialized tool or operations. After that, the fracture stimulation treatment is

* Corresponding author. Department of Chemical and Process Engineering, University of Surrey, Guildford, GU2 7XH, United Kingdom.
E-mail address: zhengchaovip@126.com (C. Zheng).

https://doi.org/10.1016/j.petsci.2021.09.011

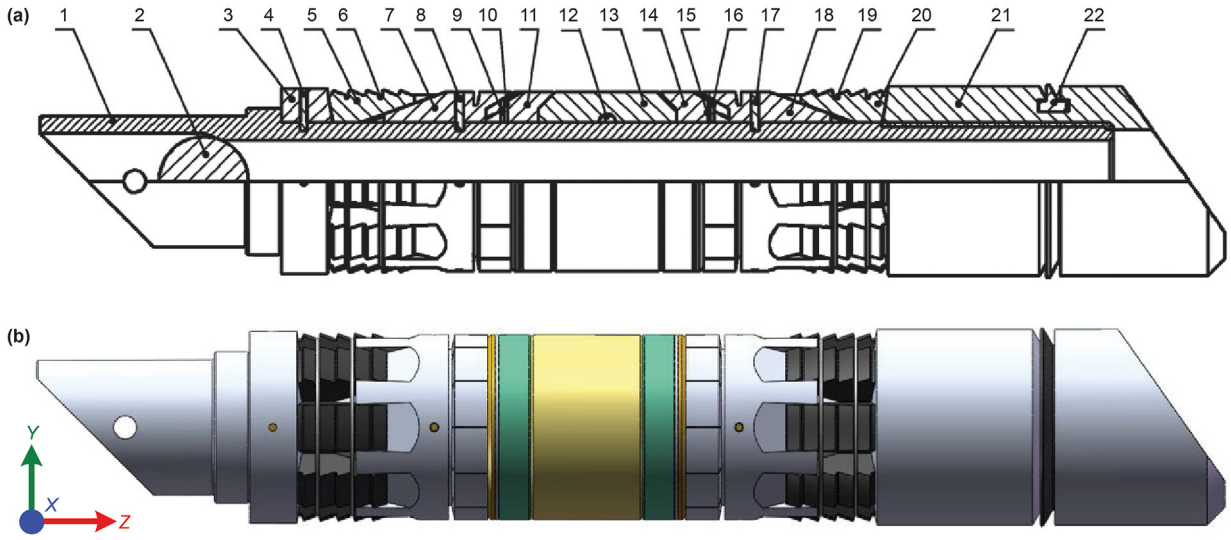

Fig. 1. 2D sketch (**a**) and 3D geometric model (**b**) for frac plug.

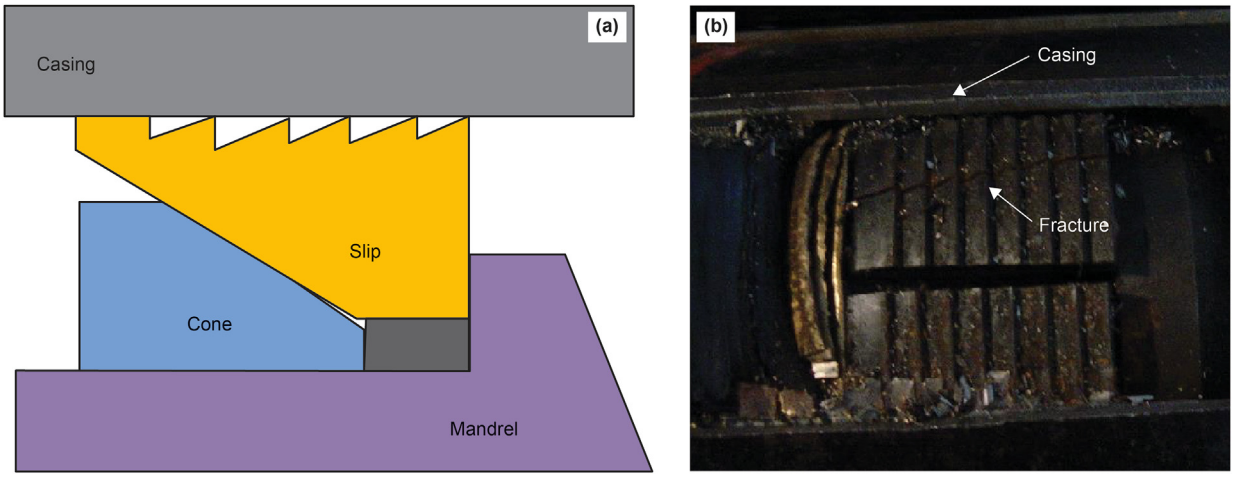

Fig. 2. Slip assembly: (**a**) slip lodged into the casing, (**b**) fracture failure.

performed. The setting of frac plug affects the sealing performance and plays a vital role during the fracturing process. When the fracturing process is completed, the frac plug should be milled out form the wellbore (Deshpande et al., 2019). Fracture failure, tool wear, and severe deformation of fracturing tools are always encountered during the fracturing process (Xi et al., 2018; Yin et al., 2018a, 2018b; Jureczka and Ochal, 2019; Lian et al., 2015; Zheng et al., 2019).

According to recent literatures, many attentions have been paid to the frac plug. Zhu et al. (2013) proposed parameter control methods for the how to properly pump the tool string composed of frac plug and perforating gun in horizontal well. Based on their control equations, the grease injection sealing pressure, minimum weight of tool string, maximum length of tool string, and pump rate can be obtained. Hu et al. (2017) studied the influence of rubber material on sealing performance of packing element in frac plug. By comparing the Mises stress, shoulder extrusion and compressive deformation magnitude of B75, A70 and E65 materials, B75 is recommended for the material of packing element. Dong et al. (2020a, b) investigated the sealing behavior of packing element for frac plug through numerical simulations and thermal aging experiments. They found that the Yeoh model is more suitable to describe deformation behavior of the packing element under high temperature. Also, the effects of parametric parameters of packing element on the sealing performance were achieved.

As mentioned above, most of the study are performed on the packing element of frac plug. However, little attention has been focused on the design optimization of the slip. Research on the design mechanism or optimization are still quite limited. Deshpande et al. (2019) performed finite element analysis (FEA) simulations to be conducted with different design formulations of composite slips to optimize the design. Their results showed that the number and material of slip button has an important impact on the slip holding capacity, which help to optimize design quickly and reduced time and cost associated with laboratory testing. Liu et al.

Table 1
Initial structural parameters of slips.

L, mm	D_w, mm	d_w, mm	α, °	β, °	γ, °
60	108	68	90	60	20

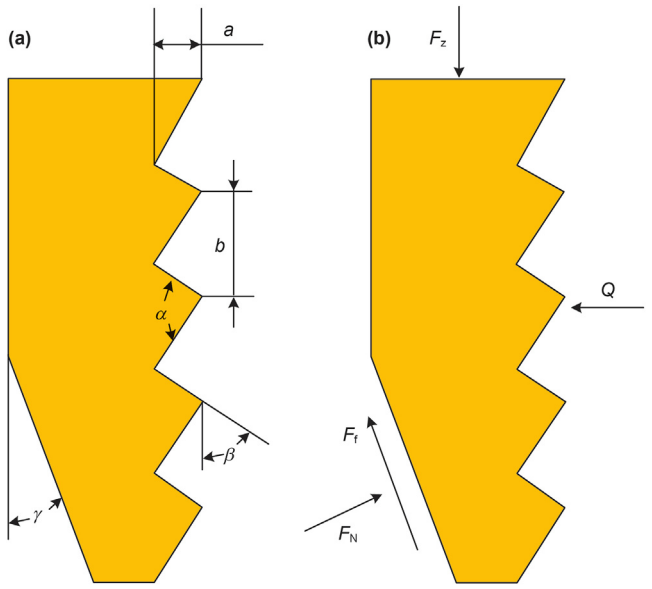

Fig. 3. Structural diagram (**a**) and force analysis (**b**) of plug slip.

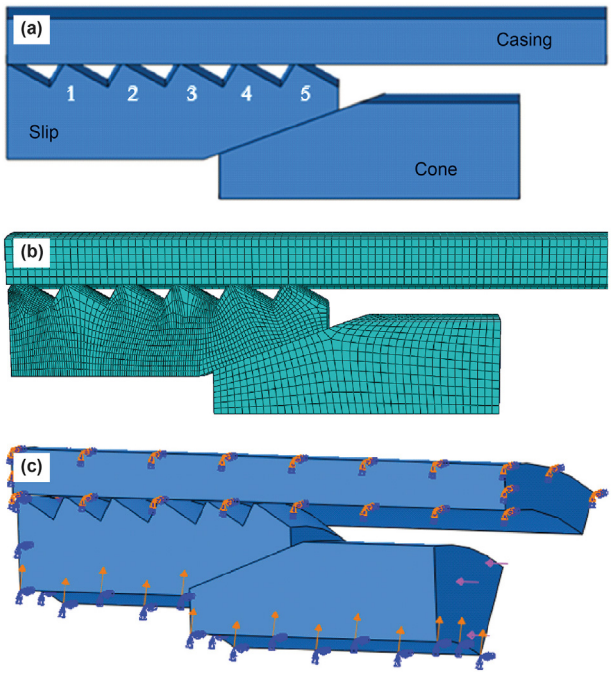

Fig. 4. Contact geometries (**a**), mesh generation (**b**), and constriction conditions (**c**).

(2020) studied on the optimization design of permanent packer slip structure. In their study, structural design of the integrated packer slip was optimized and validated by the anchoring and setting experiments, which confirmed optimized permanent slip had the advantages of low fracture strength, supplementary fracture setting performance and high reliability compared with the conventional permanent slip.

According to previous studies, the slip the quality of the setting and anchoring ability greatly affects the work reliability of the fracturing string (Deshpande et al., 2019; Liu et al., 2020). During the setting operation, the slips are forced into the casing and lock the frac plug in a specified position. Whether the slips can lodge into the casing's inner surface and hold the frac plug stably is critical to the follow-up sealing and fracturing operations. Improper selection of material and structural design may lead to possible frac plug integrity issue (Deshpande et al., 2019; Liu et al., 2020), as well as the casing integrity issues (Zhang et al., 2015; Stolyarov et al., 2020). However, the analysis of the slip contact mechanics is not sufficient. In addition, the relationship between the structural parameters and setting performance of the slip has not been revealed. This study aims to study the effects of structural parameters, including apex angle, inclination angle, and wedge angle on the setting performance of slip. These numerical results can not only provide a further insight into the setting and anchoring process, but also guide the parametric selection of plug slip and other similar components.

The presentation of this work is organized as follows. In Section 2, working principle of frac plug and numerical setup are introduced. In Section 3, obtained results are thoroughly presented and discussed. Finally, conclusions for the current study are given in Section 4.

2. Numerical details

2.1. Working principle of frac plug

So far, button slip, wicker slip, and friction slip are the main slip design for frac plug (Stolyarov et al., 2020). In this study, the wicker slip is designed to match a mandrel with an outer diameter of 68 mm and a casing pipe with an inner diameter of 139.7 mm. Based on these main dimensions, slip and rubber dimensions can be adjusted to obtain an excellent sealing performance. Fig. 1 shows the two-dimensional (2D) sketch and three-dimensional (3D) geometric model for the frac plug used in this paper. The frac plug composes of a mandrel (1), low-density ball (2), setting ring (3), shear pin (4, 8, 17), upper slip (5), slip ring (6, 19), upper cone (7), outer protective cover (9, 16), inner protective cover (10, 15), end rubber element (11, 14), O-ring (12), middle rubber element (13), lower cone (18), lower slip (20), guide shoe (21), and pump ring (22). The general setting procedure is illustrated as follows. Firstly, the frac plug is pumped to a target downhole position. Secondly, the plug is set by an explosive setting tool. Under the explosive force, the frac plug is pushed downward, and the mandrel is subjected to the upward pulling force. Then, the setting ring cuts the pin and pushes the upper and lower cone. Finally, the slips designed to interact with the cone are forced to move outward and contact the casing. Then, the hardened edges on the teeth of slips bite into the casing, locking the frac plug in place. During the setting process, the rubber elements are compressed in axial direction, which results in radial expansion to fill the annular space between the mandrel and the casing.

Table 2
Mechanical properties for contact components.

Materials	Density, kg/m^3	Elastic modulus, GPa	Yield strength, MPa	Poisson's ratio, %-
Aluminum alloy	2810	71.7	225	0.35
QT600	7200	213	600	0.286
P110	7870	206	758	0.30

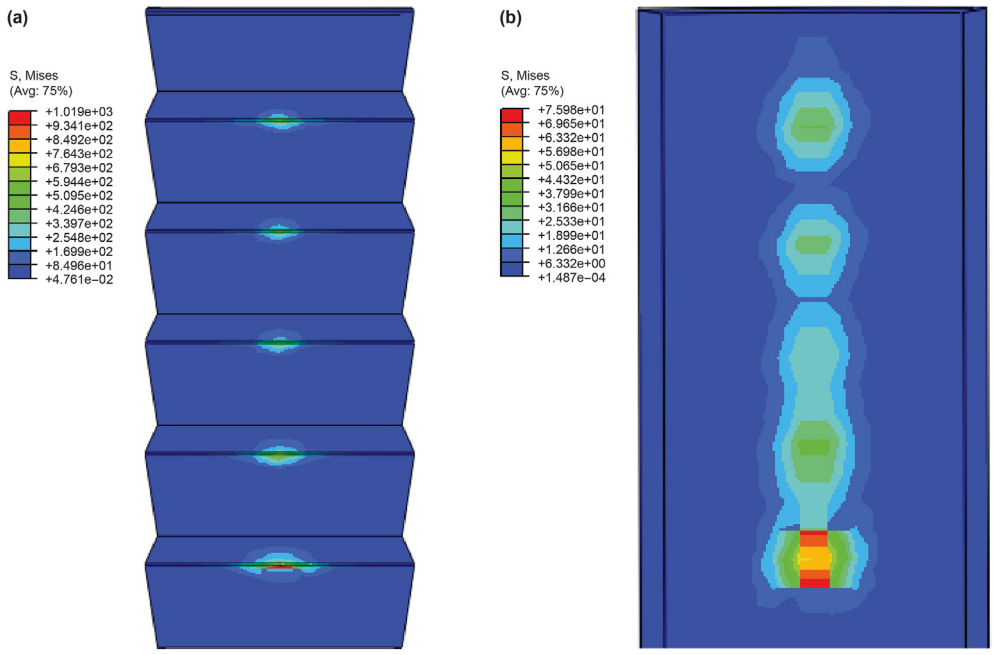

Fig. 5. Contact stress distribution for the initial slips (**a**) and casing wall (**b**).

2.2. Force analysis for slip setting

During the setting and anchoring process, the slips are forced up the corresponding cone to contact the casing. The slip lodges into the casing and locks the frac plug in a fixed position as shown in Fig. 2a. To successfully bite into the casing, the slip works under high pressure may up to 70 MPa (Deshpande et al., 2019; Liu et al., 2020; Stolyarov et al., 2020), which would always cause a high-stress concentration inside the slip, resulting in a fracture failure as depicted in Fig. 2b. The fracture failure of slip would significantly affect the setting performance of frac plug, which further impact the fracturing effects (Liu et al., 2020). Improper design of slips has been considered to be responsible for the fracture failure. Thus, it is urgent to study how the structural and processing parameters affect the setting characteristics of slips. In this study, the initial structural parameters for the slips are listed in Table 1. (L is the length of slip; D_w is the outer diameter of slip; d_w is the inner diameter of slip; α is the apex angle of slip; β is the inclination angle of slip; γ is the wedge angle of slip.)

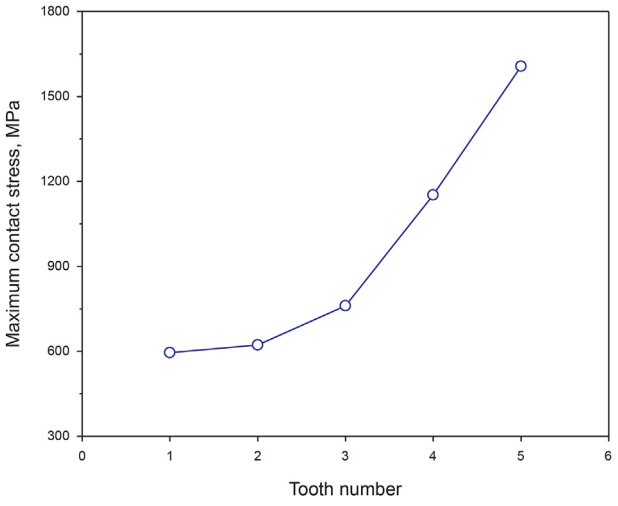

Fig. 6. Maximum stress on different teeth of slips.

Fig. 3a shows the structural diagram of plug slips. During the setting process, the forces applied on the slip are shown in Fig. 3b. It is noted that three main forces exert on the slips when the slip contact with the casing's inner wall.

With the assumption of that the multiple slips being under the same contact status of the symmetry, force equilibrium equations of each slip can be achieved as follows:

$$\left.\begin{aligned} Q &= F_N \cos\gamma - F_f \sin\gamma \\ F_Z &= F_N \sin\gamma + F_f \cos\gamma \\ F_f &= F_N \tan\phi \end{aligned}\right\} \quad (1)$$

where Q is the radial load from the inner wall of casing, F_N is the positive pressure from the cone against the slip, F_f is the friction force between cone and slip, F_Z is the axial load of the slip, W_Z is the setting load, γ is the wedge angle, ϕ is the friction angle between the slip and the cone, n is the number of slips.

From Eq. (1), the radial load and axial load on the slip can be achieved as:

$$Q = \frac{W_Z}{n \cdot \tan(\gamma + \phi)} \quad (2)$$

$$F_Z = \frac{W_Z}{n} \quad (3)$$

When the slip contacts the inner surface of the casing, the contact stress can be calculated as:

$$\sigma = \frac{Q}{A} \quad (4)$$

where σ is the contact stress of slip; A is the contact area between slip and casing wall. From the schematic diagram of slip, the contact area can be calculated using the equation below:

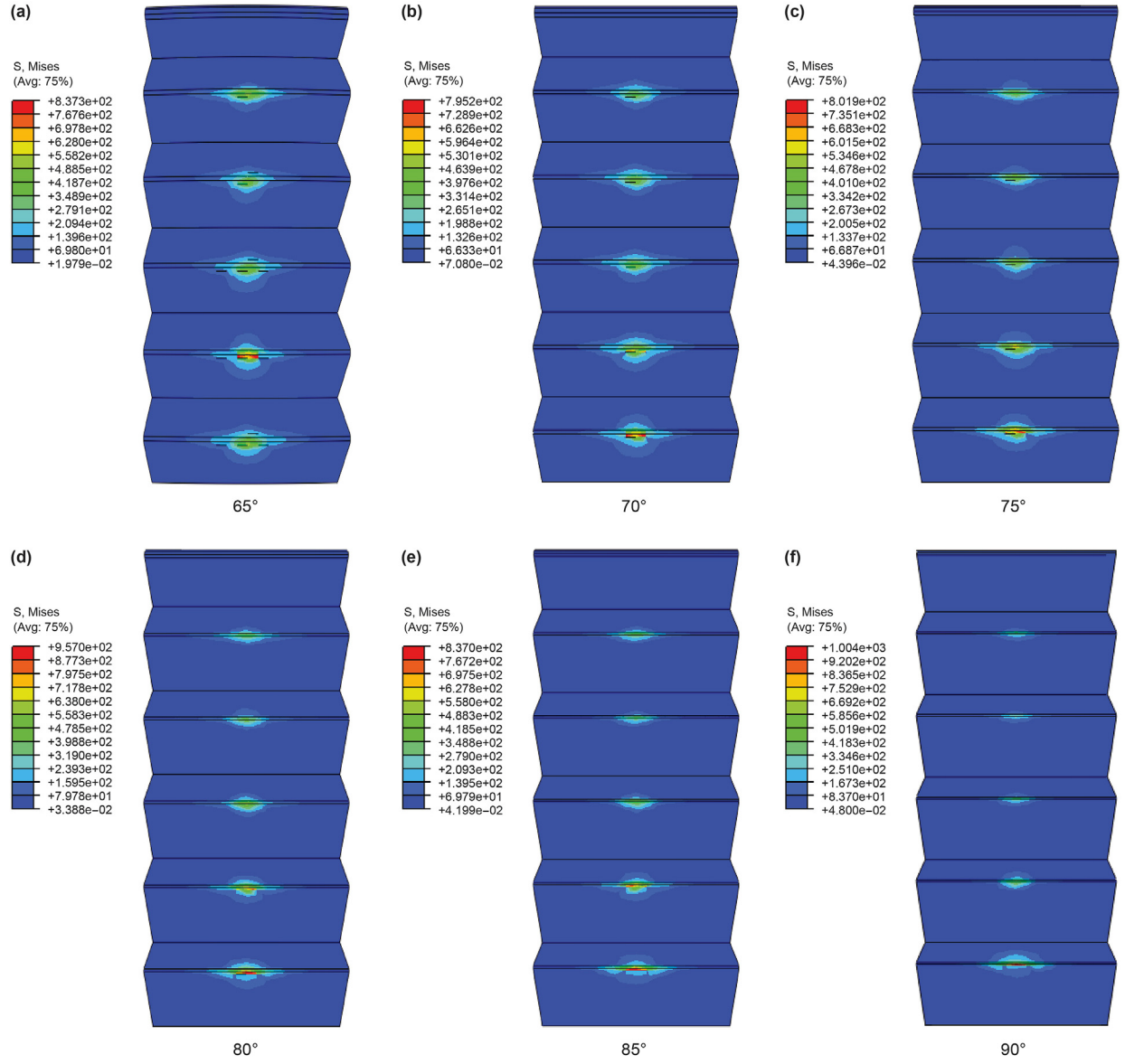

Fig. 7. Effect of apex angle on the contact stress distribution of slips.

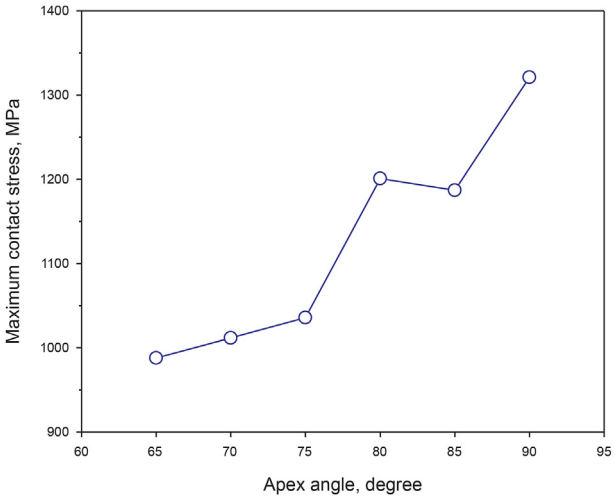

Fig. 8. Maximum contact stress under different apex angles.

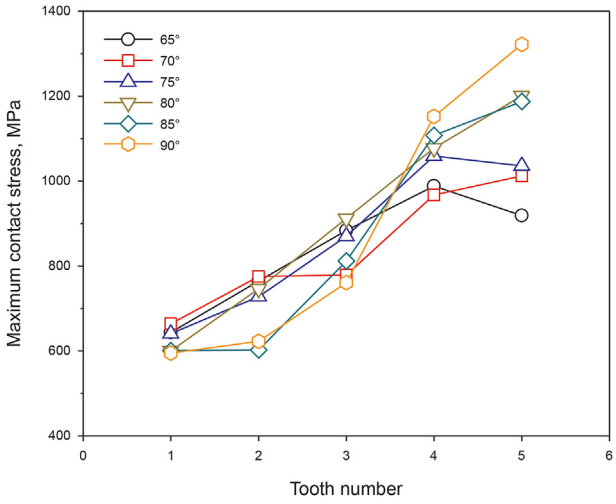

Fig. 9. Maximum contact stress of tooth under different apex angles.

$$A = ma\frac{\theta\pi D}{360}\left(\frac{1}{\tan\beta} + \tan\left(\alpha+\beta-\frac{\pi}{2}\right)\right) \tag{5}$$

where m is the number of slip tooth; a is the penetration depth of slip; θ is the circular angle of slip; D is the inner diameter of casing; α is the apex angle of slip; β is the inclination angle of slip. The number of slip tooth (m) can be achieved as:

$$m = \frac{L}{b} \tag{6}$$

where L is the length of slip; b is the width of slip tooth.

From Eqs. (4)–(6), the contact stress can be further expressed as below:

$$\sigma = \frac{360W_Z}{nma\theta\pi D\tan(\gamma+\phi)\left(\frac{1}{\tan\beta} + \tan\left(\alpha+\beta-\frac{\pi}{2}\right)\right)} \tag{7}$$

During the setting process, the shear stress can be achieved with

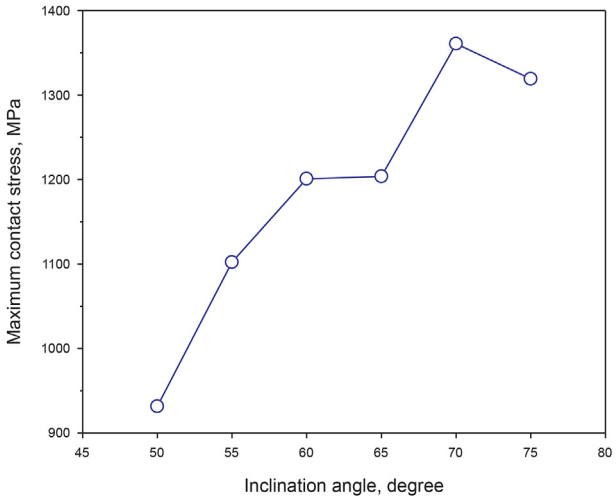

Fig. 11. Maximum contact stress under different inclination angles.

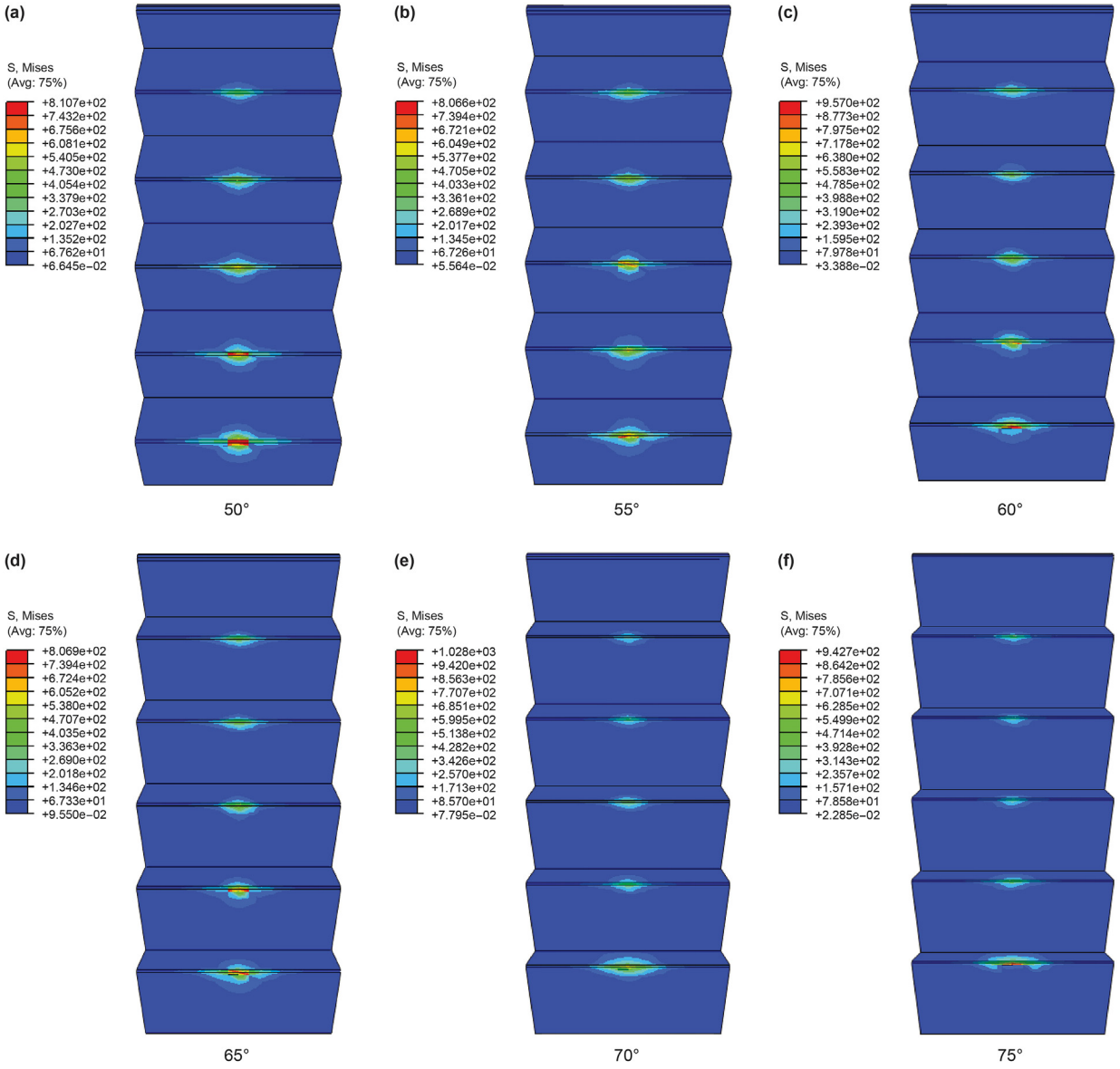

Fig. 10. Effect of inclination angle on the contact stress distribution of slips.

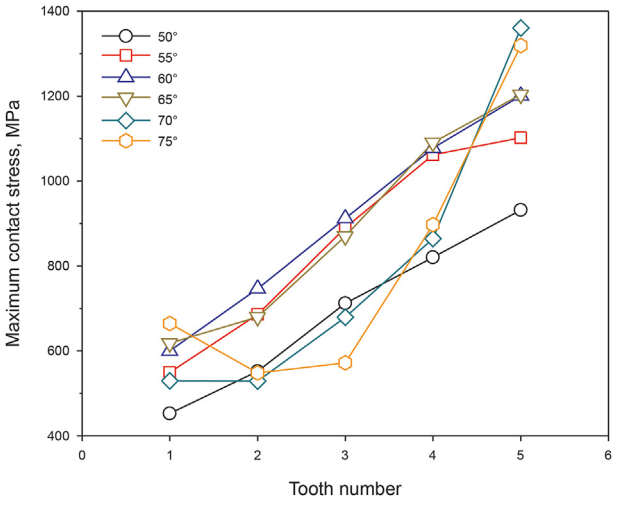

Fig. 12. Maximum contact stress of tooth under different inclination angles.

the following equation:

$$\tau = \frac{F_Z}{A} \tag{8}$$

$$\tau = \frac{360W_Z}{nma\theta\pi D\left(\frac{1}{\tan\beta} + \tan\left(\alpha + \beta - \frac{\pi}{2}\right)\right)} \tag{9}$$

where τ is the shear stress applied on the slip.

According to equations above, it can be found that structural parameters such as setting load (W_Z), tooth number of slip (m), apex angle of slip (α), and inclination angle of slip (β), and wedge angle (γ) have a critical influence on the contact characteristics of slip.

2.3. Simulation setup

The setting process mainly focuses on the contact between the slip and the casing. The ABAQUS software code is applied to

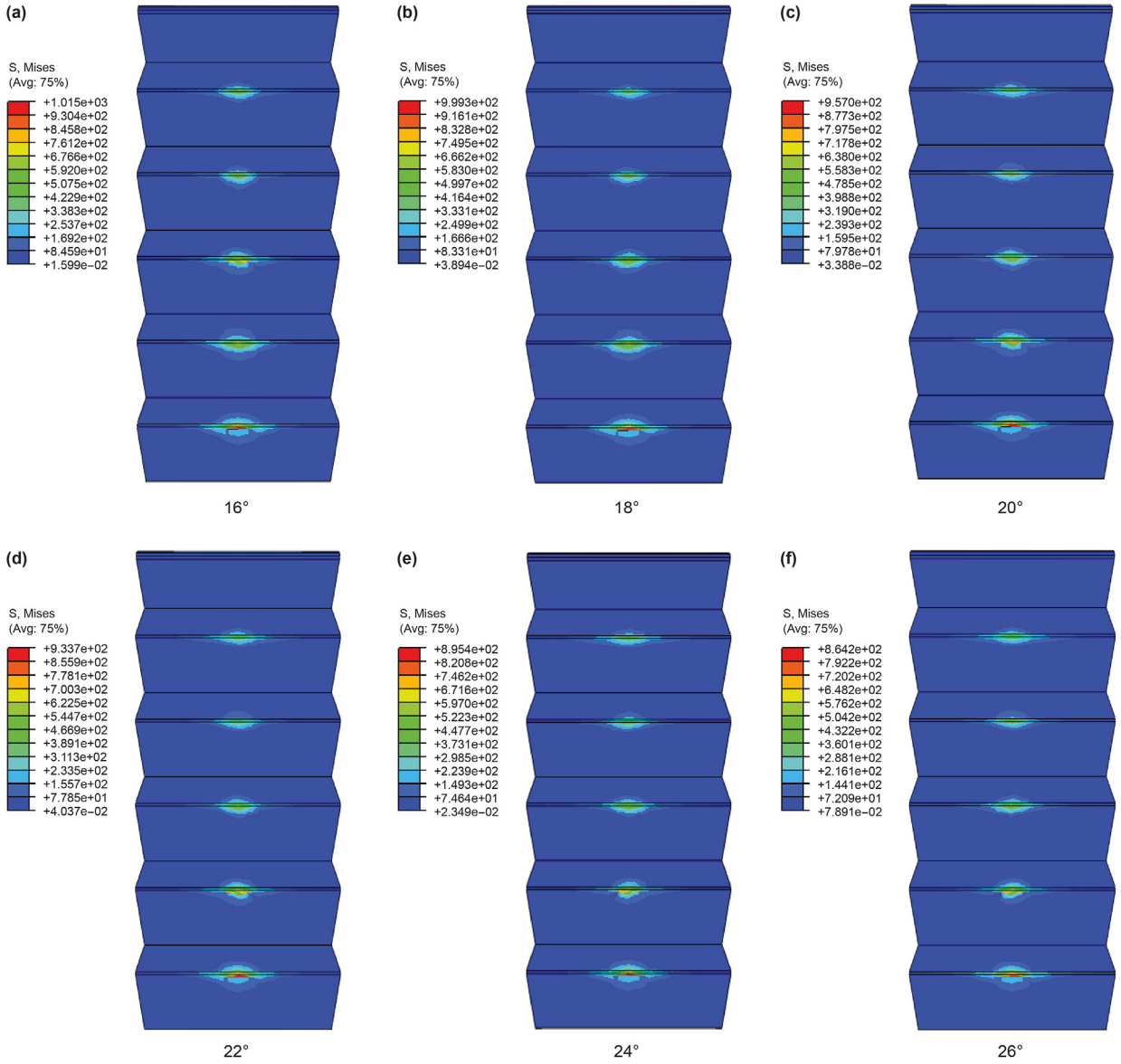

Fig. 13. Effect of wedge angle on the contact stress distribution of slips.

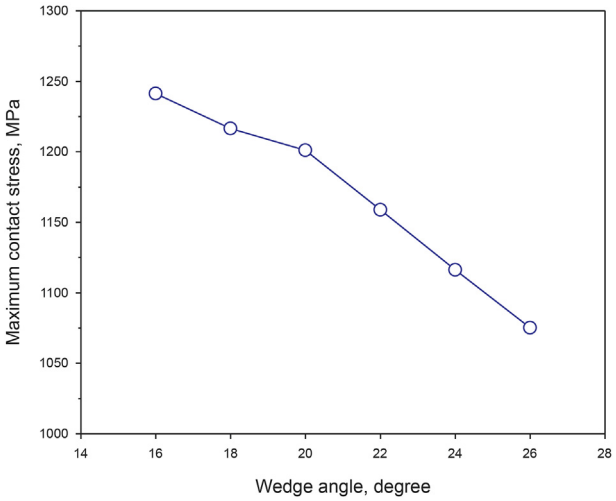

Fig. 14. Maximum contact stress under different wedge angles.

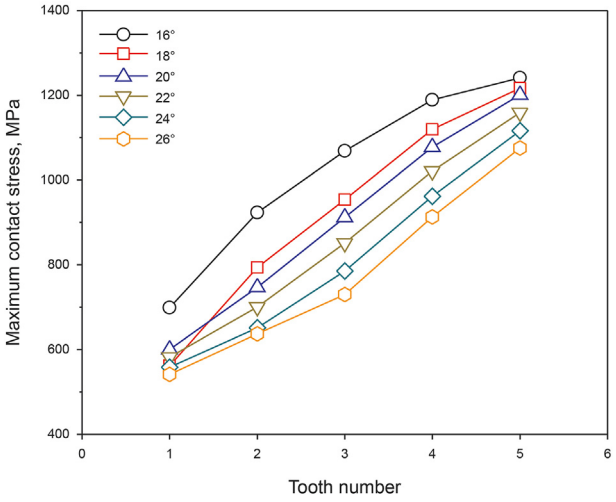

Fig. 15. Maximum contact stress of each tooth under different wedge angles.

simulate the dynamic setting process. Before the simulation, it is crucial to know the mechanical properties of material. The main components involved in the contact process are the casing, slip, and cone. The material of slip is ductile iron QT600; the cone material is high-strength aluminum alloy. The material of the casing is P110 steel. Main material properties of the contact components are listed in Table 2. The friction coefficient between the slip and the casing is 0.15, and that between the slip and the cone is 0.17. The setting load is set as 20.0 MPa in this study.

A 3D finite element contact model is established for numerical simulation. The geometric model is illustrated in Fig. 4a, and the mesh generation is presented in Fig. 4b. To accurately capture the contact details, the contact region of the slip is appropriately refined. The contact geometries are meshed with a structured grid. Grid independence is performed to obtain a proper grid number. After repeated simulations, it is found that the solution is essentially grid-independent when the grid number is larger than 27,500. According to the actual working conditions, the casing is fixed by cement; the bottom of the slip is restrained and cannot move laterally; the mandrel restrains the inner surface of the cone, and the bottom surface of the cone is exerted by the setting load, as illustrated in Fig. 4c.

3. Results and discussion

3.1. Basic setting characteristics

To better understand the basic setting process, the simulations are performed with the plug slip's initial structural parameters. Fig. 5 shows the stress contours of the slip and the casing. The stress distribution on the slip and the casing is not uniform. Stress concentration locates at the contact region between the slip and the casing. It is because that the sharp edge of slip tooth results in a small contact area and large stress. Additionally, the contact stress is different for each tooth, and the bottom area is keen to present larger stress. This is because the slip is pushed by the cone to expand outward. The bottom part of the slip is near the corresponding cone and gets a larger penetration depth on the casing, contributing to the uneven and more massive stress at the bottom area. This phenomenon is also observed by Tang et al. (2020).

To analyze the setting status between the slip and the casing, the maximum contact stress is extracted and plotted in Fig. 6. It can be seen from the figure that the maximum contact stress of the slip tooth gradually increases with the increase of the tooth number. The maximum contact stress for No. 3 to No. 5 teeth is found to be larger than the yield strength of the casing. This indicates that these slip teeth would bite into the inner surface of casing. By contrast, the contact stress of No. 1 and No. 2 tooth is much smaller.

3.2. Effect of the apex angle

As mentioned above, parameters such as the apex angle, inclination angle, and wedge angle have a crucial influence on the setting performance. By studying these parameters' effect on the contact characteristics, the slip's structural parameters can be selected. To study the effect of apex angle, slip with the apex angle of 65°, 70°, 75°, 80°, 85°, 90° are modelled and analyzed, respectively. The effect of apex angle on the contact stress of slip is presented in Fig. 7. It can be found that the contact stress concentrates around the tooth region. As shown in the figure, it can also be seen that the effective contact area of the slip gradually reduces with the increase in apex angle. At the same time, the variation of contact area between different tooth become more apparent. The variation in contact area directly reflects the contact status between the slip and the casing.

Fig. 8 shows the maximum contact stress under different apex angles. It can be concluded that maximum contact stress has a growing trend with the increase of the apex angle. Also, all the maximum contact stress is larger than the yield strength of casing, indicating an effective 'bite in' contact. The maximum contact stress of each slip tooth under different apex angles are plotted in Fig. 9. Under the same apex angle, the maximum contact stress of slip tooth generally increases with the increase of tooth number. This changing trend is also reported by Tang et al. (2020). In addition, contact stress curves under apex angles of 65°, 70°, 75°, 85°, 90° fluctuates obviously, though showing a growing trend. Among all the stress curves, the contact stress of slip under apex angle of 80° increase linearly. The stress value has a proportional relationship with the distance between the tooth and the corresponding cone. This means that each tooth has an even and functional contact with the casing. Under specific setting load, if the contact stress of different teeth fluctuated dramatically, the slip teeth are easy to destroy and affect the setting performance. Therefore, the apex angle of 80° is selected to achieve a stable and better setting performance.

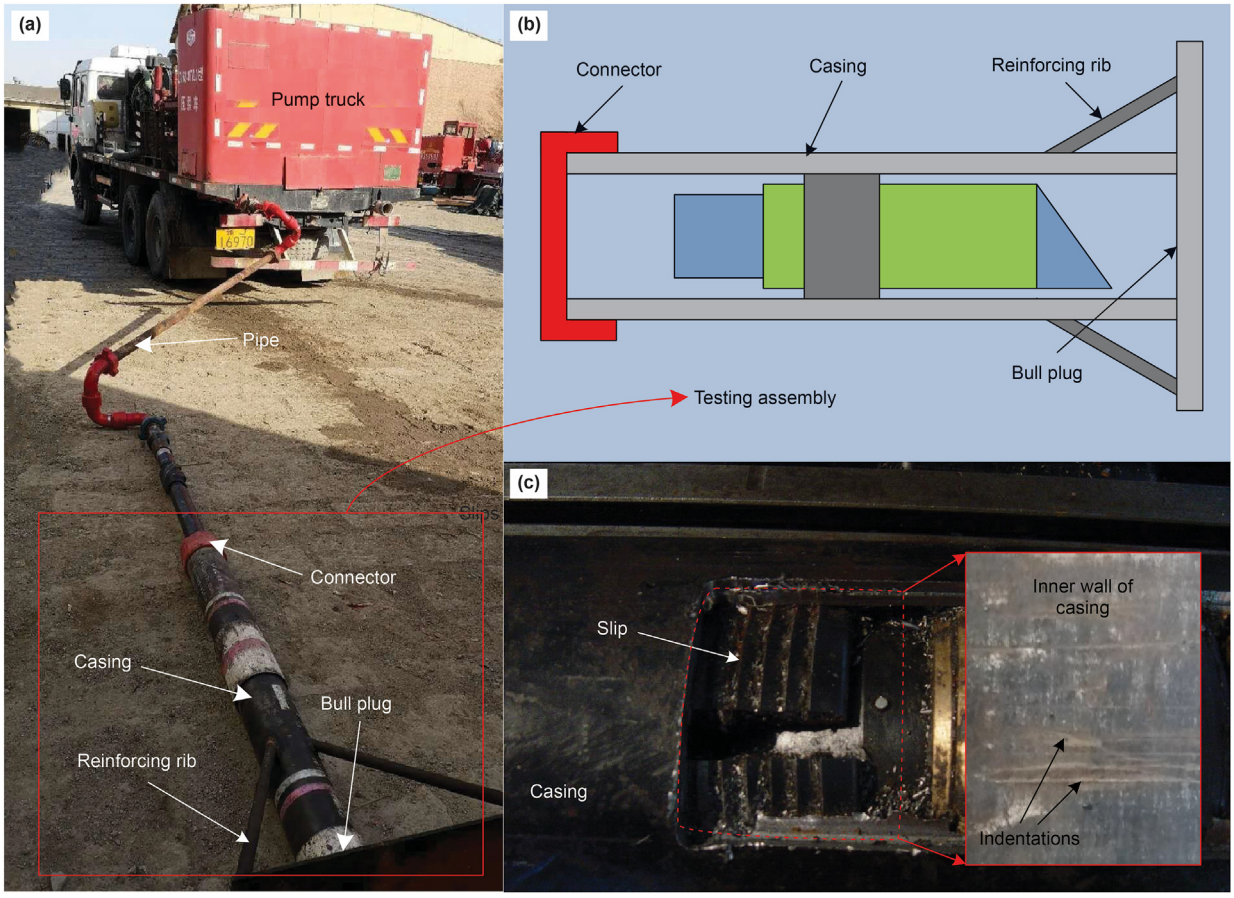

Fig. 16. Setting experiment: (**a**) full-scale setup, (**b**) test assembly, and (**c**) Assembly after test.

3.3. Effect of the inclination angle

To compare the influence of inclination angle on the setting performance, models with an inclination angle of 50°, 55°, 60°, 65°, 70°, and 75° are simulated, respectively. Fig. 10 shows the contact stress contour of slip with different inclination angles. The contact area varies with the change in inclination angle. It is interesting to observe that the contact area for different tooth varies dramatically under the inclination angle of 70° and 75°, which arises from a worse contact between the slip and the casing.

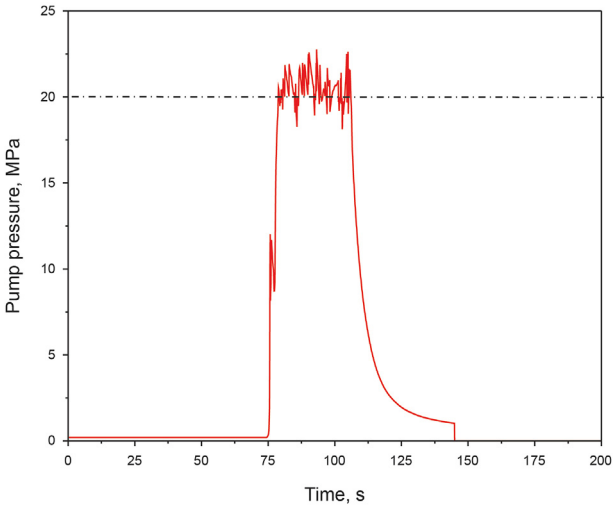

Fig. 17. Pump pressure curve during setting experiment.

Fig. 11 shows the maximum contact stress under different inclination angles. In the figure, the contact stress generally increases with the increase of inclination angle, which is beneficial to form an excellent contact. Fig. 12 plots the maximum contact stress for each tooth under different inclination angles. Under low inclination angle, each tooth's contact stress varies smoothly, indicating a better contact status. Under a high inclination angle, the contact stress for each tooth varies dramatically, which may be attributed to the uneven contact. Among all stress curves, the contact stress under inclination angle of 60° presents approximately linear growth, which reflects the best contact status. Therefore, 60° is the selected inclination angle during slip design.

3.4. Effect of the wedge angle

The wedge angle of the slip also has an essential influence on the contact performance of slip. According to the schematic diagram of slip, small wedge angles can increase the contact stress of the slip, but the small wedge angle will require a larger pushing distance of the corresponding cone. The pushing distance would directly affect the setting process. To explore the effect of wedge angle on the setting characteristics, the wedge angle of 16°, 18°, 20°, 22°, 24°, and 26° are investigated, respectively. Fig. 13 shows the contact stress contours of slip under different wedge angles. It can be seen in the figure that the distribution of contact stress is similar under

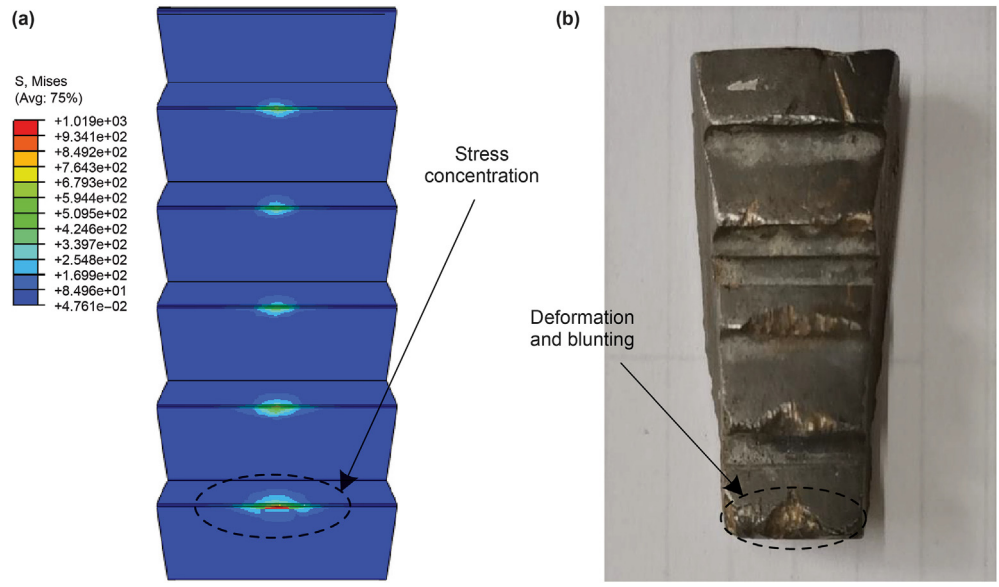

Fig. 18. Slip after setting: (**a**) numerical result and (**b**) experimental result.

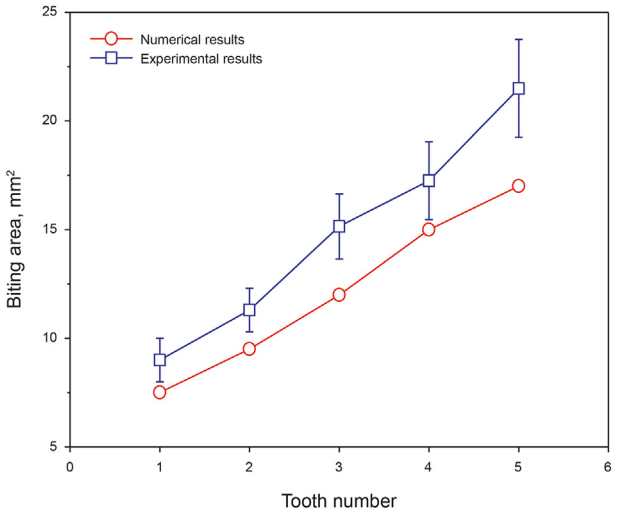

Fig. 19. Biting area on the casing for numerical and experimental results.

different wedge angles. However, the maximum contact stress varies under different wedge angles.

The maximum contact stress of the slip is plotted in Fig. 14. The maximum contact stress decreases dramatically with the increase in wedge angle. This means that the contact between the slip and the casing become worse and weak under the high wedge angle.

Fig. 15 presents the contact stress of each tooth under different wedge angles. In the figure, the contact stress under different wedge angles changes similarly. The contact stress increases with the rise in tooth number. Under the angle of 16°, maximum contact stress from No. 1 to No. 5 tooth are all larger than the yield strength of casing material, which indicates that all the teeth can successfully lodge into the casing and lock the frac plug in place. Therefore, wedge angle of 16° should be considered for the slip design.

Based on the above analyses, the apex angle, the inclination angle, and the wedge angle of packer slip are preferably selected as 80°, 60°, and 16°, respectively.

3.5. Experimental validation

To validate the numerical model, full-scale setting experiment of frac plug with selected structural parameters for the slip is conducted. The experimental rig consists of a fracturing truck, pipeline, connector, pressure gauge, frac plug assembly, and casing, as shown in Fig. 16a. The fracturing pump truck (LTJ5240TYL70, Lantong, China) can provide a maximum pump pressure up to 70 MPa. The tested frac plug is installed in the casing (outer diameter of 139.7 mm) as presented in Fig. 16b.

After all the parts are connected and checked correctly, the pump is turned on. The pump pressure is recorded by a pressure recording module with a sampling frequency of 600 Hz and a precision of 0.1 MPa. Fig. 17 plots the pump pressure curve during the setting and anchoring process of frac plug. It can be seen that the fluid pressure gradually increases to the desired testing value of 20.0 MPa. Then, the pump pressure is maintained for about 30 s to make the frac plug set sufficiently. Besides, the pump pressure is found to fluctuate. The fluctuation can be attributed to the changing contact status of components during the setting and anchoring stage of the slip (Liu et al., 2020). When the setting process finished, the pump is turned off, and the pump pressure quickly drop to zero again. After the setting experiment is completed, a window is milled on the casing for observing the setting status of various components. Noticeable indentations are found on the casing's inner surface where each tooth is set, as shown in Fig. 16c. This phenomenon indicates that the slip teeth successfully lodge in the casing.

Fig. 18 presents the visual comparison of slip between numerical and experimental results. The teeth of slip present severe plastic deformation due to stress concentration at the contact region (see Fig. 18b). Maximum deformation locates at the lower tooth, which is observed in both the numerical and experimental results. Furthermore, the sharp edges of teeth get blunting after biting into the casing. However, no fracture failure appears on the surface of slip.

When the contact stress is larger than the yield strength, plastic deformation would occur. Therefore, an effective biting area can be obtained by counting the element area. The biting area of casing can be obtained by splitting the casing and measuring the area of

indentations. Fig. 19 presents the comparison of the biting area on the casing wall for numerical results and experimental results. For both the numerical and experimental results, the biting area increases with the increase of tooth number. The teeth near the cone would generate a larger biting depth and area, which is consistent with the reports of Cai et al. (2013) and Stolyarov et al. (2020). Furthermore, the experimental results are approximately 21.3% larger than the numerical results. This can be explained that material behavior and contact status are complex under high pump pressure (Liu et al., 2020). The numerical model is difficult to take all the factors into account, which results in the under-estimate of the biting area. However, the experimental results still have a reasonable agreement with the numerical results, which indicates that the numerical approaches can effectively predict the setting process of plug slip, as well as the frac plug assembly.

4. Conclusions

Finite element analysis is performed to study the setting characteristics of plug slips. The influence of structural parameters such as apex angle, inclination angle, and wedge angle on the setting performance is systematically investigated. Based on the obtained results, the main conclusions for this study can be listed below:

(1) The contact stress distributes unevenly on the surface of the slip and the casing. Besides, the contact stress increases with the increase in tooth number. Stress concentration appears at the contact region due to the tooth's sharp edge. During the setting, the maximum contact stress of certain teeth is larger than the yield strength of the casing.
(2) With the increase of the apex angle and inclination angle, the maximum contact stress increases dramatically. However, the maximum contact stress decreases with the rise of the wedge angle. Based on the comprehensive analyses, the apex angle, inclination angle, and wedge angle are selected as 80°, 60°, and 16°, respectively.
(3) The experimental results show that the slip with selected parameters can set successfully under a setting load of 20.0 MPa. Additionally, teeth of slip get blunt and appear severe plastic deformation at the contact region, consistent with the numerical results. Comparison of the biting area indicates that the experimental results are about 21.3% larger, which still have a reasonable agreement with the numerical results.

Acknowledgments

The authors gratefully acknowledge the financial support from the National Major Science and Technology Projects of China (Grant No. 2017ZX05072), the Royal Society Newton International Fellowships (Grant No. NIF/R1/181640), and the Marie Skłodowska-Curie Individual Fellowships under European Union's Horizon 2020 research and innovation programme (Grant No. 840264).

List of symbols

L	The length of slip, mm
D_w	The outer diameter of slip, mm
d_w	The inner diameter of slip, mm
Q	The radial load from the inner wall of casing, N
F_N	The positive pressure from the cone against the slip, N
F_f	The friction force between the cone and the slip, N
F_Z	The axial load of the slip, N
W_Z	The setting load, N
n	The number of slips
A	The contact area between the slip and the casing wall, mm^2
m	The number of slip tooth
a	The penetration depth of slip, mm
b	The width of slip tooth, mm
D	The inner diameter of casing, mm

Greek letters

α	The apex angle of slip, degree
β	The inclination angle of slip, degree
γ	The wedge angle of slip, degree
θ	The circular angle of slip, degree
ϕ	The friction angle between the slip and the cone, degree
σ	The contact stress of slip, MPa
τ	The shear stress applied on the slip, MPa

Abbreviations

FEA	Finite element analysis
2D	Two-dimensional
3D	Three-dimensional

References

Ai, C., Li, X., Zhang, J., Jia, D., Tan, W.J., 2018. Experimental investigation of propagation mechanisms and fracture morphology for coalbed methane reservoirs. Petrol. Sci. 15, 815–829. https://doi.org/10.1007/s12182-018-0252-z.
Cai, W.B., Li, Z.M., Zhang, X.L., Zhang, B., Zhang, Q., 2009. Horizontal well fracturing technology for reservoirs with low permeability. Petrol. Explor. Dev. 36 (1), 80–85. https://doi.org/10.1016/S1876-3804(09)60112-9.
Cai, M., Cao, Y., Wang, X., Dou, Y., 2013. Analysis of interaction between HTHP completion Packer's slip and the casing wall. AMM 423–426, 866–870. https://doi.org/10.4028/www.scientific.net/AMM.423-426.866.
Castro, L.A., Johnson, C.C., Simpkins, D., Gandikota, R., Ring, L., Thacker, C.W., 2013. Targeted annular hydraulic fracturing using CT-enabled frac sleeves: a case history from Montana's bakken formation. In: SPE Annual Technical Conference and Exhibition, 30 September-2 October, New Orleans. https://doi.org/10.2118/166511-MS. Louisiana, USA.
Demarchos, A.S., Economides, M.J., Diyashev, I.R., Svaykin, V.A., 2005. Analysis of the performance of hydraulic fracturing treatments and quantum design improvements. In: SPE European Formation Damage Conference, 25–27 May. Sheveningen, The Netherlands. https://doi.org/10.2118/94643-MS.
Deshpande, K.M., Simpkins, D.R., Gandikota, R.V., Ring, L., 2012. Fracturing completion system optimization through advanced hydraulic modeling. In: SPE Russian Oil and Gas Exploration and Production Technical Conference and Exhibition. https://doi.org/10.2118/160552-RU, 16–18 October, Moscow, Russia.
Deshpande, K.M., Mirasdar, S.P., Mhaskar, N.A., Joshi, R.P., 2019. Composite frac plug design optimization for efficient hydraulic fracturing operations. In: SPE Eastern Regional Meeting. https://doi.org/10.2118/196606-MS, 15–17 October, Charleston, West Virginia, USA.
Dong, J.N., Yuan, G.J., Wang, X.Y., Chen, M., Jin, Y., Zeng, C., Zaman, M., 2020. Experimental study of multi-timescale crack blunting in hydraulic fracture. Petrol. Sci. https://doi.org/10.1007/s12182-020-00479-1.
Dong, L.L., Li, K., Zhu, X.H., Li, Z.Q., Zhang, D.P., Pan, Y., 2020. Study on high temperature sealing behavior of packer rubber tube based on thermal aging experiments. Eng. Fail. Anal. 108, 104321. https://doi.org/10.1016/j.engfailanal.2019.104321.
Ge, H.K., Yang, L., Shen, Y.H., Ren, K., Meng, F.B., Ji, W.M., Wu, S., 2015. Experimental investigation of shale imbibition capacity and the factors influencing loss of hydraulic fracturing fluids. Petrol. Sci. 12, 636–650. https://doi.org/10.1007/s12182-015-0049-2.
Haddad, M., Kamy, S., 2015. Simulation of hydraulic fracturing in quasi-brittle shale formations using characterized cohesive layer: stimulation controlling factors. J. Unconv. Oil Gas Resour. 9, 65–83. https://doi.org/10.1016/j.juogr.2014.10.001.
Hejl, K.A., Madding, A.M., Morea, M., 2007. Extreme multistage fracturing improves vertical coverage and well performance in the lost hills field. SPE Drill. Complet. 22, 326–333. https://doi.org/10.2118/101840-PA.
Hu, G., Zhang, P., Wang, G.R., Zhang, M., Li, M., 2017. The influence of rubber material on sealing performance of packing element in compression packer. J. Nat. Gas Sci. Eng. 38, 120–138. https://doi.org/10.1016/j.jngse.2016.12.027.
Jureczka, M., Ochal, A., 2019. Numerical analysis and simulations of contact problem with wear. Comput. Math. Appl. 77, 2980–2988. https://doi.org/10.1016/j.camwa.2018.08.044.
Lian, Z.H., Yu, H., Lin, T.J., Guo, J.H., 2015. A study on casing deformation failure during multi-stage hydraulic fracturing for the stimulated reservoir volume of horizontal shale wells. J. Nat. Gas Sci. Eng. 23, 538–546. https://doi.org/10.1016/j.jngse.2015.02.028.
Liu, Z., Zhang, L., Wang, F., Li, S., Wang, P., Cai, M., Han, L.L., Ma, Y.Y., Ma, Z.L., Yan, B.X., 2020. Study on optimization design of permanent packer slip

structure. J. Fail. Anal. Prev. https://doi.org/10.1007/s11668-020-01063-w.
Mahmoodi, S., Abbasi, M., Sharifi, M., 2019. New fluid flow model for hydraulic fractured wells with non-uniform fracture geometry and permeability. J. Nat. Gas Sci. Eng. 68, 102914. https://doi.org/10.1016/j.jngse.2019.102914.
Rosine, R.S., Blanco, I.L., Bailey, M., 2008. Comparison of computational fluid dynamics of erosion in coiled tubing to field and test data. In: SPE/ICoTA Coiled Tubing and Well Intervention Conference and Exhibition. The Woodlands, Texas, USA. https://doi.org/10.2118/113619-MS, 1–2 April.
Rutqvist, J., Rinaldi, A.P., Cappa, F., Moridis, G.J., 2013. Modeling of fault reactivation and induced seismicity during hydraulic fracturing of shale-gas reservoirs. J. Petrol. Sci. Eng. 107, 31–44. https://doi.org/10.1016/j.petrol.2013.04.023.
Shaw, J., 2011. Benefit and application of a surface-controlled sliding sleeve for fracturing operations. In: SPE Annual Technical Conference and Exhibition. https://doi.org/10.2118/147546-MS, 30 October-2 November, Denver, Colorado, USA.
Stolyarov, S., Casanova, G., Xu, Y.Q., Deng, G.J., Holmes, K., Gomez, R., Young, A., 2020. How much can you afford to ignore casing failure during hydraulic fracturingš the search for a non damaging frac plug. In: SPE Annual Technical Conference & Exhibition, pp. 26–29. https://doi.org/10.2118/201715-MS. October, Virtual.
Suri, Y., Islam, S.Z., Hossain, M., 2019. A new CFD approach for proppant transport in unconventional hydraulic fractures. J. Nat. Gas Sci. Eng. 70, 102951. https://doi.org/10.1016/j.jngse.2019.102951.
Tan, P., Jin, Y., Yuan, L., Xiong, Z.Y., Hou, B., Chen, M., Wan, L.M., 2019. Understanding hydraulic fracture propagation behavior in tight sandstone–coal interbedded formations: an experimental investigation. Petrol. Sci. 16, 148–160. https://doi.org/10.1007/s12182-018-0297-z.
Tang, Y., Sun, P., Wang, G.R., Li, W., 2020. Analysis of pressure-bearing performance and optimization of structural parameters of the slip in a compression packer. Sci. Prog. 103, 1–19. https://doi.org/10.1177/0036850419881106.
Tong, S.Y., Gu, M., Singh, R., Mohanty, K.K., 2019. Proppant transport in foam fracturing fluid during hydraulic fracturing. J. Petrol. Sci. Eng. 182, 106279. https://doi.org/10.1016/j.petrol.2019.106279.
Tsai, K.C., Degaleesan, S.S., Fonseca, E.R., Lake, E., 2012. Advanced computational modeling of proppant settling in water fractures for shale gas production. SPE J. 18, 50–56. https://doi.org/10.2118/151607-PA.
Vishkai, M., Gates, I., 2019. On multistage hydraulic fracturing in tight gas reservoirs: Montney Formation, Alberta, Canada. J. Petrol. Sci. Eng. 174, 1127–1141. https://doi.org/10.1016/j.petrol.2018.12.020.
Wang, J.L., Feng, L.Y., Steve, M., Tang, X., Gail, T.E., Mikael, H., 2015. China's unconventional oil: a review of its resources and outlook for long-term production. Energy 81, 31–42. https://doi.org/10.1016/j.energy.2014.12.042.
Xi, Y., Li, J., Liu, G.H., Cha, C.Q., Fu, Y.Q., 2018. Numerical investigation for different casing deformation reasons in Weiyuan-Changning shale gas field during multistage hydraulic fracturing. J. Petrol. Sci. Eng. 163, 691–702. https://doi.org/10.1016/j.petrol.2017.11.020.
Yin, F., Han, L.H., Yang, S.Y., Deng, Y., He, Y.M., Wu, X.R., 2018a. Casing deformation from fracture slip in hydraulic fracturing. J. Petrol. Sci. Eng. 166, 235–241. https://doi.org/10.1016/j.petrol.2018.03.010.
Yin, F., Xiao Han, Y., Xing, L.H., Wu, R., 2018b. Quantifying the induced fracture slip and casing deformation in hydraulically fracturing shale gas wells. J. Nat. Gas Sci. Eng. 60, 103–111. https://doi.org/10.1016/j.jngse.2018.10.005.
Zhang, D.R., Li, D., Kong, C.Y., 2012. Design of new-pattern sidetracking setting tool and finite element analysis for slips. Oil Field Equipment 41 (10), 69–71 (in Chinese).
Zheng, F.Y., Zhang, M.D., Zhang, W.Q., Tan, R.L., Guo, X.D., 2019. On the deformed tooth contact analysis for forged bevel gear modification. Mech. Mach. Theor. 135, 192–207. https://doi.org/10.1016/j.mechmachtheory.2019.01.024.
Zheng, C., Liu, Y.H., Wang, H.X., Zhu, H.Y., Liu, Z.K., Cai, B.P., Shen, Y., 2016. Numerical study on improving the erosion life of ball seat for oil and gas reservoir fracturing. Eng. Fail. Anal. 60, 188–198. https://doi.org/10.1016/j.engfailanal.2015.11.050.
Zheng, C., Liu, Y.H., Wang, H.X., Zhu, H.Y., Ji, R.J., Liu, Z.K., Shen, Y., 2015. Research on the effect of gas nitriding treatment on the wear resistance of ball seat used in multistage fracturing. Mater. Des. 70, 45–52. https://doi.org/10.1016/j.matdes.2014.12.050.
Zhu, X.X., Xue, S.F., Tong, X.H., 2013. Parameter control methods for the pumping tool string composed of perforating gun and fracturing plug in a horizontal well. Petrol. Explor. Dev. 40 (3), 398–404. https://doi.org/10.1016/S1876-3804(13)60050-6.